

Analysis of the fusion mechanism in synthesis superheavy element 119 via $^{54}\text{Cr}+^{243}\text{Am}$ reaction

B.M. Kayumov^{1,4}, O.K. Ganiev^{1,2,5}, A.K. Nasirov^{1,3,*} and G.A. Yuldasheva¹

¹*Institute of Nuclear Physics, Uzbekistan Academy of Science, 100214 Tashkent, Uzbekistan*

²*College of Engineering, Akfa University, 100095 Tashkent, Uzbekistan*

³*Joint Institute for Nuclear Research, 141980 Dubna, Russia*

⁴*New Uzbekistan University, 100007 Tashkent, Uzbekistan*

⁵*Faculty of Physics, National University of Uzbekistan, 100174 Tashkent, Uzbekistan*

(Dated: November 5, 2021)

The combined dinuclear system (DNS) and statistical model implanted in KEWPIE2 have been used to study the prospects for the synthesis of a superheavy element (SHE) with $Z = 119$ in the $^{54}\text{Cr}+^{243}\text{Am}$ fusion reaction. The method of calculation has been verified by description of the evaporation residue cross sections measured for the $^{48}\text{Ca}+^{243}\text{Am}$ reaction. The calculated results of the partial and total cross sections for the complete fusion, quasifission, fast fission and evaporation residues formation for both reactions are discussed.

I. INTRODUCTION

In modern nuclear physics, the fusion of massive nuclei is one of the main research topics due to the great motivation in the synthesis of new superheavy elements (SHEs) [1–9]. Remarkable recent progress in the synthesis of new SHEs has been achieved using of the ^{48}Ca projectile with the transactinides [4–8]. Various theoretical and experimental studies have been carried out to study the nuclear fusion process of the formation of SHE aiming to two main aspects: the first reason is to find out and analyze the mechanism of synthesis of SHE, the second is to search for the best projectile-target combination and a suitable incident energy for obtaining new SHEs and their isotopes. In particular, the evaporation residue (ER) cross section strongly depends on the incident energy and the projectile-target combination. Therefore, the study of such dependences is interesting and especially useful when trying to synthesize new SHEs with $Z > 118$. This is important due to the fact that the ER cross section of fusion reactions with these nuclei becomes very small, and the excitation functions are very narrow. This circumstance causes extremely difficulties in synthesis of the heaviest superheavy elements in experiments.

In order to determine the best conditions for formation of SHE, several experiments were carried out to study the influence of the entrance channel on the ER cross section [10–12]. The isospin effect of the target nucleus has been recently investigated on the ER cross section [13]. In some laboratories, the experiments aimed to synthesize SHEs with $Z = 119$ and 120 were performed via hot fusion reactions [14, 15]. To estimate the fusion probability correctly it is necessary to distinguish pure fusion-fission products from the quasifission products [16–21]. Since the experimental characteristics of the quasifission and fusion-fission processes [22] may be similar. Therefore, it

is important a better understanding the dependence of the complete fusion process on the entrance channel to distinguish mechanisms creating fusion-fission and quasifission fragments which can have overlap in the observed mass distributions.

In general, many theoretical models have been developed and applied to interpret experimental data by estimating the evaporation residue cross section. On one hand, the synthesis mechanism of SHE needs to be elucidated [23–35]. Various approaches are devoted to calculating the fusion probability of the colliding nuclei, as well as analyzing the distribution of quasifission fragments [28, 36–38]. On the other hand, in order to produce the new SHEs, or their isotopes far from the island of stability of the chemical elements, it is necessary to estimate the corresponding incident energy and the best projectile-target combination.

The extended nuclear landscape allows us to investigate the nuclear structure of SHE and the nuclear reaction mechanism. To search for the optimal condition of synthesis, the influence of the entrance channel [28, 39–41] and the isospin of heavy colliding nuclei [42, 43] on the evaporation residual cross section have been studied systematically in many works. In particular, in some works [24, 28, 44–49] predictions were made of a possible method for the synthesis of new SHEs with $Z = 119$ and 120.

On the whole, the final cross section for the formation of SHE depends on two factors: 1) the fusion probability in the entrance channel; 2) competition between the fission process and the evaporation of neutrons in the output channel. In case of the massive nuclei interaction, the capture of the projectile-nucleus by the target-nucleus does not lead directly to their complete fusion as in case of the collision of the light nuclei. Alternative channel to complete fusion is quasifission process when the DNS formed at capture breaks down after multinucleon process due to presence of the intrinsic fusion barrier against transfer all nucleons of the lighter fragment to the heavy one. The maximum of the mass-charge distribution of the quasifission products is concentrated near

* nasirov@jinr.ru

yield of the magic nuclei having the proton and/or neutron magic numbers. Experiments with massive nuclei show that quasifission is dominant channel in comparison with complete fusion, particularly in cold fusion reactions [20, 50]. Therefore, the fusion probability becomes very sensitive to the entrance channel. The competition between the fission process and the evaporation of neutrons at each stage of the decay process will significantly reduce the survival probability of the final SHE. Therefore, accurate calculations and predictions of these cross sections are very important since experimenters can choose the optimal combinations of projectile and target, as well as the favorable beam energy at which the synthesis of SHE is possible. In particular, in order to study the formation of evaporation residues, it is important to analyze the role of the entrance channel characteristics, such as incident energy and orbital angular momentum which are responsible at formation the angular momentum distribution of the excited compound nucleus. Thus, this research could be useful in planning future experiments.

The main goal of this paper is to examine the possibility of the formation of the 119th superheavy element as a result of the $^{54}\text{Cr} + ^{243}\text{Am}$ reaction within the framework of the developed DNS model. In particular, we have calculated the capture, fusion, and ER cross sections for the $^{48}\text{Ca} + ^{243}\text{Am}$ and $^{54}\text{Cr} + ^{243}\text{Am}$ reaction based on the developed DNS model. We have demonstrated the role of the orbital angular momentum in the formation of a compound nucleus.

II. THEORETICAL DESCRIPTION FOR THE FORMATION OF SHN

The formation of SHE is a result of the complicated dynamical process with the multinucleon transfer between interacting nuclei. Therefore, it is very important to better understand the different steps of the reaction mechanism of SHE formation. Theoretically, from our point of view, the SHE synthesis process can be divided into several reaction stages. A schematic diagram of the stages preceding the formation of evaporation residues is shown in Fig. 1. The first stage is a competition between deep-inelastic collision (incomplete momentum transfer) and capture process (full momentum transfer). At this reaction stage, the colliding nuclei overcome the Coulomb barrier and come into close contact with the overlapping surfaces of the nuclei. As a function of the initial collision energy and impact parameter one of above mentioned events takes place. If after dissipation of the sufficient part of the relative kinetic energy the system is able overcome the Coulomb barrier from the inside to outside the deep-inelastic collision (I) occurs (see Fig.1) and if the residual part of the kinetic energy is not enough to overcome the Coulomb barrier the system is trapped into potential well of the nucleus-nucleus interaction (see Fig. 2 in Ref. [39]). The last case is called capture and full momentum transfer takes place (II). The difference between

capture and deep-inelastic collisions depends on whether the path of relative motion has been trapped into the potential well or not. Consequently, the lifetime of DNS formed at capture is longer in comparison the one of DNS formed in the deep-inelastic collisions. This competition strongly depends on the collision energy and the impact parameter (angular momentum of relative motion). This fact allows to separate the products of these two different reaction mechanisms. In the second stage of the reaction, the evolution of DNS can end with the CN formation with excitation energy E_{CN}^* in an equilibrium state, or it can arrive at two fragments without reaching the state of CN. The last process is called quasifission (II) (see Fig. 1). The quasifission occurs when the DNS prefers to break down into two fragments rather than becoming a fully equilibrated CN. The quasifission is the main hindrance to the CN formation during the evolution of DNS in reactions with massive nuclei, since this process is dominant relative to the complete fusion. This channel of evolution of DNS due to multinucleon transfer is shown as channel II. Quasifission products can have characteristics similar to those of nuclear fission. For example, the mass distributions of the fusion-fission and quasifission products may overlapped parts and the total kinetic energy of quasifission fragments is close to the total kinetic energy of fission fragments. The third stage is the process of formation of a rotationally excited mononucleus, which occurs due to the transfer of all nucleon from the light fragment to heavy nucleus. Rotation of a non-equilibrium mononucleus causes decreasing its fission barrier. Consequently, at a certain value of the orbital angular momentum, the fission barrier disappears completely. In this case, the non-equilibrium mononucleus becomes unstable and undergoes fission from some excited state. The splitting of a mononucleus before reaching its equilibrium state is called fast-fission (III), as a result of which binary mass- symmetric fragments are formed. This process leads to the formation of binary products (see Fig. 1), which causing hindrance for the heated and rotating mononucleus to be de-excited and transformed into CN. So, fast fission depends on the splitting of the mononucleus before reaching equilibrated CN, if $L_{CN} > L_f$ [51], where L_f is a value at which fission barrier of CN disappears at the given excitation energy. It is well known that the increase of the CN excitation energy also decreases of the fission barrier appeared due to shell effects in massive nuclei. This phenomenon is related with the washing out the shell effects in the heated nuclei.

Recall that the quasifission process can occur for all L_{DNS} values of the DNS. This is one of the main differences between fast-fission and quasifission. The fourth stage is that the binuclear system evolves from a tangent configuration to the CN formation, which can be estimated by the probability of merging. In the last stage, the excited CN undergoes to the last competition between fission into two fragments (IV) and cooling by the emission of neutrons, and the result of this competition is estimated by the survival probability. It should be

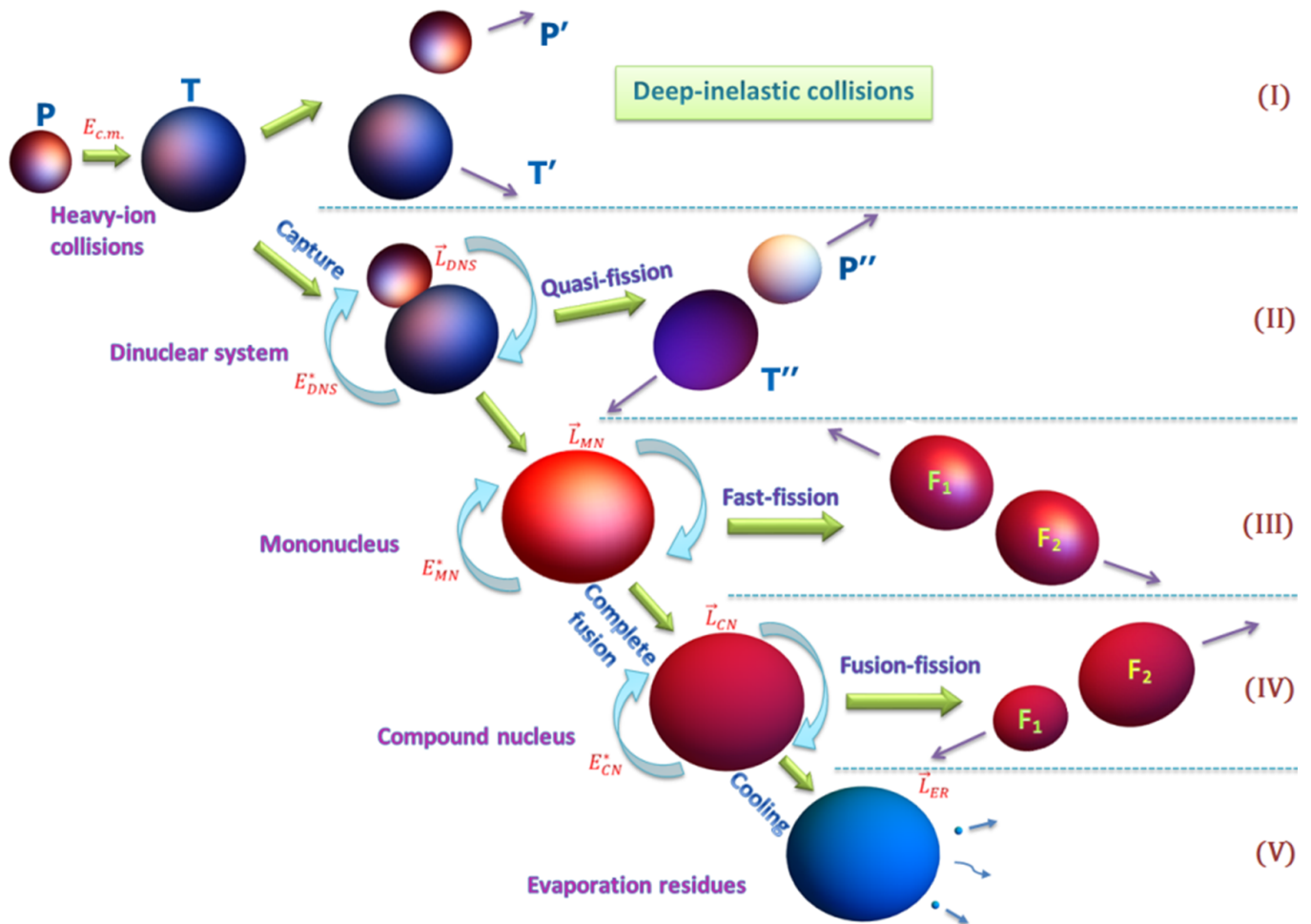


FIG. 1. (Color online) Schematic diagram of the reaction mechanisms causing hindrance at formation of the superheavy nuclei in heavy-ion collisions. The multinucleon transfer reactions and fission (I–IV) leading to the formation of binary or fission-like fragments, which compete in the way to the ER formation (superheavy nuclei). I. deep-inelastic collision (not full momentum transfer) of the initial projectile P and target T nuclei; II. Quasifission (full momentum transfer) products P'' and T''; III. Fast fission (fission of non-equilibrated mononucleus) products F₁ and F₂; IV. Fusion-fission (fission of compound nucleus) products F₁ and F₂.

stressed that a very small evaporation residue cross section is obtained for the SHN production (V).

III. OUTLINE OF THE APPROACH

The study of the main processes taking place in heavy-ion collisions near the Coulomb barrier energies is based on calculations of the incoming path of the projectile nucleus and finding the capture probability for the interaction with different orientation angles of the axial symmetry axis of a deformed nuclei and at the given value of the collision impact parameter [39, 52–54]. Also, the surface vibrations of the nuclei, which are spherical in the ground state are taken into consideration. The final results are averaged over all orientation angles (α_1 and α_2) of the axial symmetry axis of deformed nuclei relative to the beam direction or vibrational states of the spheri-

cal nuclei. These procedures are presented in Subsection III C of this work.

A. Capture

The capture process in heavy-ion collisions (i.e., capture of a projectile nucleus by a target nucleus) is closely related to the peculiarities of interacting nuclei and the entrance channel effects. This is due to the fact that the nucleus-nucleus potential depends on the shape and orientation angles of the symmetry axis of the interacting nuclei and plays an important role in determining the DNS fate. In generally, a DNS consists of two basic degrees of freedom that lead to capture: (i) the intrinsic degree of freedom due to the exchange of nucleons between the projectile nucleus and the target, and (ii) the collective degree of freedom from relative motion be-

tween the two nuclei leads to capture. In this context, the capture cross section is one of primary interest to experimentalists and theorists studying the reaction mechanism in heavy-ion collisions since only full momentum transfer to the intrinsic and collective degrees of freedom from the relative motion is the beginning of the way of the compound nucleus formation [53–55]. The capture cross section is an observable quantity and, at the same time, one of the important components in the synthesis of superheavy nuclei. In this regard, in order to successfully predict a possible way to synthesize the new SHEs, it is very important to carefully examine the capture process associated with an accurate description of the capture cross section measurements.

Typically, capture requires two conditions to be met:

1. The initial energy of the projectile nucleus in the center-of-mass system $E_{c.m.}$ must be sufficient to reach the potential well by overcoming or tunneling through the barrier at a relative distance R in the entrance channel;
2. Some of the relative kinetic energy must be dissipated for the dinuclear system to induce trapping in the potential well.

This condition depends on the shape and orientation angles (α_1 and α_2) of the symmetry axis of the interacting nuclei and orbital angular momentum ($L = \ell\hbar$) which determine the size of the potential well, and the intensity of the friction forces that cause the kinetic energy of the relative motions to dissipate into the internal energy of two interacting nuclei. In our approach, the height of the inner barrier of the well of the nucleus-nucleus poten-

tial is called the quasifission barrier which is a hindrance against decay of dinuclear system. An alternative process of quasifission in the evolution of the DNS is the complete fusion of its constituent fragments. Thus, the capture cross section for a given relative energy in the center of mass system ($E_{c.m.}$) and angular momentum (ℓ) is the sum of the cross sections for complete fusion, quasifission and fast fission:

$$\begin{aligned} \sigma_{cap}(E_{c.m.}, \ell; \alpha_1, \alpha_2) &= \sigma_{fus}(E_{c.m.}, \ell; \alpha_1, \alpha_2) \\ &+ \sigma_{qfis}(E_{c.m.}, \ell; \alpha_1, \alpha_2) \\ &+ \sigma_{ffis}(E_{c.m.}, \ell; \alpha_1, \alpha_2). \end{aligned} \quad (1)$$

The appearance of the term $\sigma_{ffis}(E_{c.m.}, \ell; \alpha_1, \alpha_2)$ representing a contribution of the fast fission process in nucleus-nucleus collisions is discussed in Section IV.

The capture cross section is determined by the number of partial waves which lead the path of the total energy of colliding nuclei to be trapped in the well of the nucleus-nucleus potential after dissipation of a sufficient part of the initial kinetic energy [54]. The size of the potential well decreases with increasing orbital angular momentum ℓ .

The capture cross section is calculated by the following formula:

$$\begin{aligned} \sigma_{cap}(E_{c.m.}, \ell; \alpha_1, \alpha_2) &= \frac{\lambda^2}{4\pi} \sum_{\ell=0}^{\ell_d} (2\ell + 1) \\ &\times \mathcal{P}_{cap}^{\ell}(E_{c.m.}, \ell; \alpha_1, \alpha_2), \end{aligned} \quad (2)$$

where λ is the de Broglie wavelength of the entrance channel and $\mathcal{P}_{cap}^{\ell}(E_{c.m.}, \ell; \alpha_1, \alpha_2)$ is the capture probability which depends on the collision dynamics:

$$\mathcal{P}_{cap}^{(\ell)}(E_{c.m.}, \ell, \{\beta_i\}) = \begin{cases} 1, & \text{if } \ell_m < \ell < \ell_d \text{ and } E_{c.m.} > V_B, \\ 0, & \text{if } \ell < \ell_m \text{ or } \ell > \ell_d \text{ and } E_{c.m.} > V_B \\ \mathcal{P}_{tun}^{(\ell)}(E_{c.m.}, \ell, \{\beta_i\}), & \text{for all } \ell \text{ if } E_{c.m.} \leq V_B \end{cases} \quad (3)$$

where V_B is the barrier of the nucleus-nucleus potential in the entrance channel; β_i are parameters of the nuclear shape deformation; ℓ_m and ℓ_d are the minimum and maximum values of the orbital angular momentum ℓ leading to capture at the given collision energy. This means that the values of ℓ leading to capture can form a “window” determined by the size of the potential well of the nuclear-nuclear potential. The fact is that the coefficient of friction is not so high enough to trap the projectile in a potential well. Thus, the boundary values ℓ_{min} and ℓ_d of the partial waves leading to capture depend on the dynamics of collision and they are determined by solving the equations of motion for the relative distance R and orbital angular momentum ℓ [39, 56]. $\mathcal{P}_{tun}^{(\ell)}$ is probability of the barrier penetrability which is calculated by the

improved WKB formula by Kemble et al [57]:

$$\mathcal{P}_{tun}^{(\ell)}(E_{c.m.}, \{\beta_i\}) = \frac{1}{1 + \exp[2K(E_{c.m.}, \ell, \{\beta_i\})]}, \quad (4)$$

where

$$K(E_{c.m.}, \ell, \{\beta_i\}) = \int_{R_{in}}^{R_{out}} \sqrt{\frac{2\mu}{\hbar^2} (V(R, \ell, \{\beta_i\}) - E_{c.m.})} dR. \quad (5)$$

R_{in} and R_{out} are inner and outer turning points which were estimated by $V(R) = E_{c.m.}$.

B. Potential energy surface. The driving potential

The potential energy of a heavy nuclear configuration plays a crucial role in understanding the evolution of collisions of nuclei. Generally, the potential energy surface (PES) is very important in the DNS model, which provides information about the optimal projectile-target combination, the optimal excitation energy, and influences the fusion probability significantly. The PES is calculated as a function of the mass and charge numbers of its fragments, orbital angular momentum (ℓ) of collision and relative distance R between their mass centres (see Fig. 2):

$$U(Z_i, A_i, \ell, R, \beta_i, \alpha_i) = Q_{gg} + V_N(Z_i, A_i, \ell, R, \beta_i, \alpha_i) - V_{rot}^{CN}(\ell) \quad (i = 1, 2), \quad (6)$$

where $\beta_i (i = 1, 2)$ represent quadrupole deformations of the colliding nuclei, $Q_{gg} = B_1 + B_2 - B_{CN}$ is the reaction energy balance that is used to determine the excitation energy of CN; B_1 , B_2 , and B_{CN} are the binding energies of the interacting nuclei and CN, respectively, which are obtained from the nuclear mass tables in Refs. [58, 59]. And also nucleus-nucleus potential (V_N) consists of three

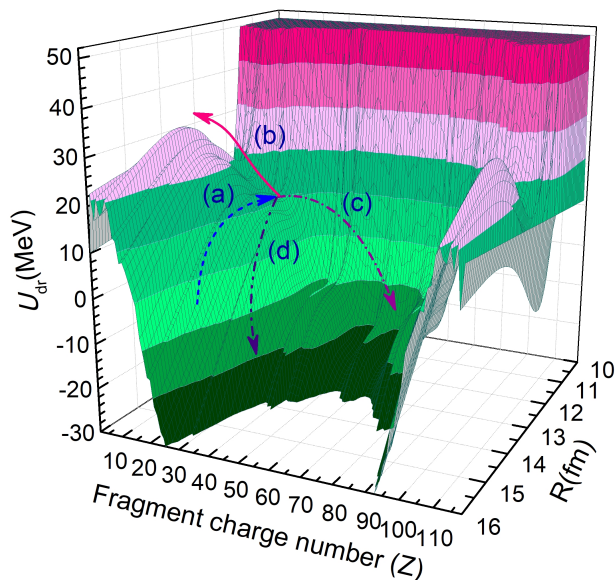


FIG. 2. (Color online) Potential energy surface calculated as a function of the relative distance between the interacting nuclei and fragment charge number for the $^{54}\text{Cr}+^{243}\text{Am}$ reaction leading to the CN $^{297}\text{119}$. Arrow (a) shows the capture path in the entrance channel; arrow (b) shows the direction of the complete fusion by multinucleon transfer from the light nucleus to the heavy one; (c) and (d) arrows show the directions of decay of the DNS into mass symmetric and asymmetric quasifission channels, respectively.

parts:

$$V_N(Z_i, A_i, \ell, R, \beta_i, \alpha_i) = V_{nucl}(Z_i, A_i, \ell, R, \beta_i, \alpha_i) + V_{Coul}(Z_i, A_i, \ell, R, \beta_i, \alpha_i) + V_{rot}(Z_i, A_i, \ell, R, \beta_i, \alpha_i), \quad (7)$$

where V_{nucl} , V_{Coul} , and V_{rot} are the nuclear, Coulomb, and rotational potentials, respectively. The methods of calculation of these three parts of the nucleus-nucleus potential as a function of the orientation angles of the symmetry axis of the colliding nuclei are presented in Appendix A of Refs. [39, 56]. If the colliding nuclei are deformed then the parameters ($\beta_i, i = 1, 2$) of their deformation and orientation angles (α_i) of axial symmetry axis are included into consideration.

Fig. 2 shows the PES calculated at $\ell = 0$ for $^{54}\text{Cr}+^{243}\text{Am}$ reaction leading to the CN $^{297}\text{119}$. The arrow (a) shows the capture path in the entrance channel; the arrow (b) shows the direction of complete fusion by multinucleon transfer from the light nucleus to the heavy one; the arrows (c) and (d) show the directions of decay of the DNS into mass symmetric and asymmetric quasifission channels, respectively. Only some of the paths of the DNS evolution along the charge asymmetry axis (the solid arrow (b)) and surviving against decay along the relative distance lead to complete fusion, i.e., to the CN formation. The intrinsic barrier B_{fus}^* causing

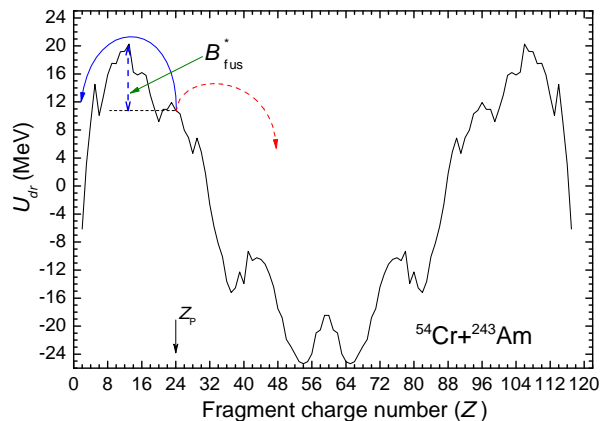


FIG. 3. (Color online) Calculated driving potential for the DNS $^{297}\text{119}$ formed in the $^{54}\text{Cr}+^{243}\text{Am}$ reaction versus the charge number of its fragment. B_{fus}^* is the intrinsic fusion barrier causing a hindrance to complete fusion. The solid curved arrow shows the way to complete fusion while the dashed curved arrow shows evolution of DNS to quasifission channels.

a hindrance to complete fusion and quasifission barrier B_{qf} preventing a decay of DNS are determined from the landscape of PES. The intrinsic barrier B_{fus}^* is estimated from the peculiarities of the driving potential which is formed as a curve connecting the minima of the well of the nucleus-nucleus potential corresponding to the different mass asymmetry configuration of dinuclear system formed at capture (see Fig. 3). In Fig. 3, the B_{fus}^* value for the DNS configuration $^{54}\text{Cr}+^{243}\text{Am}$ is demonstrated. As a quasifission barrier B_{qf} the depth of the well of the nucleus-nucleus potential is used. These quantities are

used in calculation of the fusion probability P_{CN} of the interacting DNS fragments.

C. Fusion

In calculation of the fusion probability the change of the mass and charge distributions during capture is included, *i.e.* the fusion probability of the colliding nuclei is taken as a sum of the competition of complete fusion and quasifission at different charge asymmetry from the symmetric configuration Z_{sym} of DNS up to configuration corresponding to the maximum value of the driving

potential Z_{max} :

$$P_{CN}(E_{c.m.}, \ell, \{\beta_i\}) = \sum_{Z_{sym}}^{Z_{max}} D_Z(E_Z^*, \ell) P_{CN}^{(Z)}(E_Z^*, \ell, \{\beta_i\}). \quad (8)$$

The weight function $D_Z(E_Z^*, \ell)$ is the charge distributions probability in the DNS fragments which is determined by solution of the transport master equation [55]. The fusion probability $P_{CN}^{(Z)}(E_Z^*, \ell, \{\beta_i\})$ for the DNS fragments with the charge configuration Z rotating with the orbital angular momentum ℓ is calculated as the branching ratio $P_{CN}^{(Z)}(E_Z^*, \ell; \{\alpha_i\})$ of widths related to the overflowing over the quasifission barrier $B_{qf}(Z)$ at a given mass asymmetry, over the intrinsic barrier $B_{fus}(Z)$ on mass asymmetry axis to complete fusion [60]:

$$P_{CN}^{(Z)}(E_Z^*, \ell) \approx \frac{\Gamma_{fus}^{(Z)}(B_{fus}^{(Z)}, E_Z^*, \ell)}{\Gamma_{(qf)}^{(Z)}(B_{qf}^{(Z)}, E_Z^*, \ell) + \Gamma_{(fus)}^{(Z)}(B_{fus}^{(Z)}, E_Z^*, \ell) + \Gamma_{sym}^{(Z)}(B_{sym}, E_Z^*, \ell)}, \quad (9)$$

where Γ_{fus} , Γ_{qf} and Γ_{sym} are corresponding widths determined by the level densities on the barriers $B_{fus}^{(Z)}$, $B_{sym}^{(Z)}$ and $B_{qf}^{(Z)}$ are the intrinsic fusion, symmetric fission and quasifission barriers; E_Z^* is the the excitation energy of DNS with the charge asymmetry Z and it is calculated by formula

$$E_Z^*(A, \ell) = E_{c.m.} - V(Z, A, R_m, (\ell)) + \Delta Q_{gg}(Z, A), \quad (10)$$

where $V(Z, A, R_m, (\ell))$ is the minimum value of the potential well $V(Z, A, R, \ell)$ at R_m ; $\Delta Q_{gg}(Z, A) = B_1 + B_2 - B_P - B_T$ is included to take into account the change of the intrinsic energy of DNS due to nucleon transitions during its evolution along mass and charge asymmetry axes, where B_P , B_T , B_1 and B_2 are binding energies of the initial (“P” and “T”) and (“1” and “2”) interacting fragments at the given time t of interaction. The width Γ_i of the decay through the corresponding barriers B_i is determined by the level densities on the barriers [39]:

$$\Gamma_i^{(Z)}(B_i^{(Z)}, E_Z^*, \ell) \approx \frac{\rho_i(E_Z^* - B_i^{(Z)}, \ell)}{\rho_i(E_Z^*, \ell)} T_Z, \quad (11)$$

where $T(Z) = 3.46 \sqrt{E_Z^*/(A_P + A_T)}$ is the effective temperature of the DNS having the charge asymmetry Z . As a level density $\rho(E_Z^*, \ell)$ is calculated by the expression [37]:

$$\rho(E_Z^*, \ell) = \left[\frac{g^2}{g_1 g_2} \right]^{1/2} \frac{g}{6^{3/4} (2gE_Z^*)^{5/4}} \exp \left[2(aE_Z^*)^{1/2} \right], \quad (12)$$

where $2g = g_1 + g_2$ and $\pi^2 g_i / 6 = A_i / 11 \text{ MeV}^{-1}$.

The partial fusion excitation function is determined by the partial capture cross sections σ_{cap}^ℓ and fusion probabilities $P_{CN}(E_{c.m.}, \ell, \{\beta_i\})$ of DNS for the heavy collisions with the given orbital angular momentum ℓ :

$$\sigma_{fus}(E, \ell, \alpha_1, \alpha_2) = \sigma_{cap}(E, \ell; \alpha_1, \alpha_2) P_{CN}(E, \ell; \alpha_1, \alpha_2). \quad (13)$$

Partial fusion cross section is found by averaging over all values of the orientation angles α_1 and α_2 symmetry axis of the deformed projectile and target nuclei:

$$\sigma_{fus}(E_{CN}^*, \ell) = \int_0^{\pi/2} \int_0^{\pi/2} \sigma_{fus}(E_{CN}^*, \ell; \alpha_1, \alpha_2) \times \sin \alpha_1 \sin \alpha_2 d\alpha_1 d\alpha_2. \quad (14)$$

To calculate the capture and fusion cross sections in the reactions with the nuclei of the spherical shape their surface vibrations have been considered as independent harmonic vibrations and the nuclear radius is taken to be distributed as a Gaussian distribution [61],

$$g(\beta, \alpha) = \exp \left[- \frac{(\sum_\lambda \beta_\lambda Y_{\lambda 0}^*(\alpha))^2}{2\sigma_\beta^2} \right] (2\pi\sigma_\beta^2)^{-1/2}, \quad (15)$$

where α is the direction of the spherical nucleus. For simplicity, we use $\alpha = 0$:

$$\sigma_\beta^2 = R_0^2 \sum_\lambda \frac{2\lambda + 1}{4\pi} \frac{\hbar}{2D_\lambda \omega_\lambda} = \frac{R_0^2}{4\pi} \sum_\lambda \beta_\lambda^2, \quad (16)$$

where ω_λ is the frequency and D_λ is the mass parameter of a collective mode.

As the amplitudes of the surface vibration we use deformation parameters of first excited 2^+ and 3^- states of the colliding nuclei. The values of the deformation parameters of first excited 2^+ and 3^- states are presented in Table I which are taken from Ref(s). [62] (β_2^+) and [63] (β_3^-).

Partial fusion cross section is found by averaging over values of the vibrational states β_i of the spherical nuclei:

$$\sigma_{fus}(E_{CN}^*, \ell) = \int_{-\beta_0}^{+\beta_0} \sigma_{fus}(E_{CN}^*, \ell; \beta) g(\beta) d\beta. \quad (17)$$

The partial fusion cross sections calculated by this way are used in estimations of the partial evaporation residue cross sections for the given values of the angular momentum distributions of the compound nucleus formed with the excitation energy

$$E_{CN}^*(\ell) = E_{c.m.} + Q_{gg} - V_{CN}^\ell, \quad (18)$$

where $Q_{gg} = B_P + B_T - B_{CN}$ is a reaction energy balance; V_{CN}^ℓ and B_{CN} are rotational and binding energies of the compound nucleus.

D. Evaporation residue

In the DNS approach, the partial cross sections of the CN formation are used to calculate evaporation residue (ER) cross sections at given values of the CN excitation energy E_x^* and angular momentum ℓ :

$$\sigma_{ER}^x(E_x^*) = \sum_0^{\ell_d} (2\ell + 1) \sigma_{ER}^x(E_x^*, \ell). \quad (19)$$

where, $\sigma_{ER}^x(E_x^*, \ell)$ is the partial cross section of ER formation obtained after the emission of particles from the intermediate nucleus with the excitation energy E_x^* at each step x of the de-excitation cascade by the formula [39, 42]:

$$\sigma_{ER}^x(E_x^*, \ell) = \sigma_{ER}^{x-1}(E_{x-1}^*, \ell) W_{sur}^x(E_{x-1}^*, \ell). \quad (20)$$

Here, $\sigma_{ER}^{x-1}(E_{x-1}^*, \ell)$ is the partial cross section of the intermediate excited nucleus formation at the $(x-1)$ th step and obviously, $\sigma_{ER}^{(0)}(E_{x-1}^*, \ell) = \sigma_{fus}(E_{CN}^*, \ell)$ which is calculated by (17); $W_{sur}^x(E_{x-1}^*, \ell)$ is the survival probability of the x th intermediate nucleus against fission along

the de-excitation cascade of CN. The survival probability $W_{sur}^x(E_{x-1}^*, \ell)$ is calculated by the statistical model implanted in KEWPIE2 [64], which is dedicated to the study of SHEs. In presented results, the Weisskopf approximation [65] is used to calculate neutron emission width:

$$\Gamma_n = \frac{(2S_n + 1)\mu_n}{\pi^2 \hbar^2} \int_0^{E_{CN}^* - B_n} \frac{\sigma_{inv}^n(\epsilon_n) \rho_B(E_B^*) \epsilon_n d\epsilon_n}{\rho_{CN}(E_{CN}^*)} \quad (21)$$

where $\rho_{CN}(E_{CN}^*)$ is the level density of intermediate nucleus, E_B^* is the excitation energy of the residual nucleus after the emission of a neutron, B_n is the binding energy of the neutron with the residue nucleus, S_n and ϵ_n denote the intrinsic spin of the neutron and its kinetic energy, σ_{inv}^n is the cross section for the time-reversed reaction.

In the KEWPIE2 code, the fission-decay width is estimated within the standard Bohr–Wheeler transition-state model [66]:

$$\Gamma_f^{BW} = \frac{1}{2\pi \rho_{CN}^{gs}(E_{CN}^*, J_{CN})} \int_0^{E_{CN}^* - B_f} \rho_C^{sd}(E_{sd}^*, J_{CN}) \times T_{fiss}(\epsilon_f) d\epsilon_f, \quad (22)$$

here, the excitation energy at the saddle point is equal $E_{sd}^* = E_{CN}^* - B_f - \epsilon_f$, $\rho_{CN}^{gs}(E_{CN}^*, J_{CN})$ and $\rho_C^{sd}(E_{sd}^*, J_{CN})$ are the level densities of the nucleus at the ground-state and saddle-point deformation. In the KEWPIE2 code [64], the improved state-density formula, which was first proposed in Ref. [67], has been employed to estimate various decay widths. $T_{fiss}(\epsilon_f)$ is a penetration factor which corresponds to the Hill-Wheeler transmission coefficient [68]. The fission barrier consists of a macroscopic liquid-drop component and microscopic shell correction energy component. For SHEs, the macroscopic part is relatively small, and the liquid-drop model gives the fission barriers of less than 1 MeV for $Z > 105$. The main contribution is given by the shell correction energy. However, the shell correction energies for SHEs have not yet been firmly confirmed [69]. In KEWPIE2, a shell correction factor f is introduced to account for this uncertainty [64]:

$$B_f = B_{LD} - f\delta W \quad (23)$$

where B_{LD} and δW are the liquid-drop fission barrier and the effective shell-correction energy, respectively. The liquid-drop fission barrier is estimated by using Lublin-Strasbourg Drop model [70]. The ground-state shell correction energies and the parameterizations for liquid-drop fission barrier are using the mass table of Möller et al. [59]. The dependence of the fission barrier on the excitation energy E_{CN}^* and angular momentum ℓ of the CN can be taken into account as in Ref. [21], where the correction factor f was written as $h(T)q(\ell)$,

$$h(T) = \{1 + \exp[(T - T_0)/d]\}^{-1} \quad (24)$$

TABLE I. Deformation parameters β_2 and β_3 of first excited 2^+ and 3^- states of the colliding nuclei used in the calculations in this work.

Nucleus	^{48}Ca	^{54}Cr	^{243}Am
β_2^+ [62]	0.106	0.250	0.293
β_3^- [63]	0.101	0.250	0.083

and

$$q(\ell) = \{1 + \exp[(\ell - \ell_{1/2})/\Delta\ell]\}^{-1}. \quad (25)$$

In Eq.(24) $T = \sqrt{E_{CN}^*/a}$ is nuclear temperature, $d = 0.3$ MeV is the rate of washing out the shell corrections with the temperature, $T_0 = 1.16$ MeV is the value at which the damping factor $h(T)$ is reduced by 1/2; in Eq.(25), $\Delta\ell = 3\hbar$ is the rate of washing out the shell corrections with the angular momentum, $\ell_{1/2} = 20\hbar$ is the value at which the damping factor $q(\ell)$ is reduced by 1/2. To calculate the level density parameter a , Ignatyuk's prescription [71] was used.

IV. RESULTS AND DISCUSSION

The evaporation residue cross sections for the $^{48}\text{Ca}+^{243}\text{Am}$ and $^{54}\text{Cr}+^{243}\text{Am}$ reactions have been calculated by the use of partial fusion cross sections found by Eq. (17). This way allows us to take into account the influence of the orbital angular momentum on the probability of the compound nucleus formation. It should be noted that the averaging procedures over orientation angles ($0^\circ, 15^\circ, 30^\circ, 45^\circ, 60^\circ, 75^\circ,$ and 90°) of the axial symmetry axis of the deformed nuclei ^{54}Cr and ^{243}Am by Eq. 14 and over 7 vibrational states ($-\beta_2^+, -2\beta_2^+/3, -\beta_2^+/3, 0, \beta_2^+/3, 2\beta_2^+/3, \beta_2^+$) of the spherical nucleus ^{48}Ca Eq. (17) have been performed to get the partial cross sections under discussion.

The results of the partial fusion and quasifission cross sections obtained for the $^{48}\text{Ca}+^{243}\text{Am}$ reaction are presented in Fig. 4 and 5, respectively. Two main differences are seen from these Figs: 1) the values of the quasifission cross section are more than one order larger the ones of complete fusion; 2) very wide range of the angular momentum values contribute to the formation of the quasifission products while the only values angular momentum up to $\ell = 40$ can contribute the complete fusion cross sections since the fission barrier B_f disappears at $\ell > 40$. The part of the partial cross section corresponding to complete fusion and having angular momentum distribution $\ell > 40$ can be considered as the cross section presenting the fast fission process. It should be stressed the set of DNS with the angular momentum $\ell > 40$ has survived against quasifission and such DNS transform into mononucleus but it cannot reach compound nucleus state since at this condition it has not fission barrier B_f providing possibility to have an equilibrated state.

The angular momentum distribution of the mononucleus which is a set of the DNS survived against quasifission is demonstrated in Fig. 6. The fission of mononucleus with the angular momentum $\ell > \ell_f$ is called fast fission. For the $^{48}\text{Ca}+^{243}\text{Am}$ reaction it occurs at $\ell \geq 40$. The damping the fission barrier is calculated by Eqs.(25) and (24). At last the cross sections for the yield of the evaporation residues after emission of 2, 3 and 4 neutrons (2n, 3n and 4n channels) in competition against fission

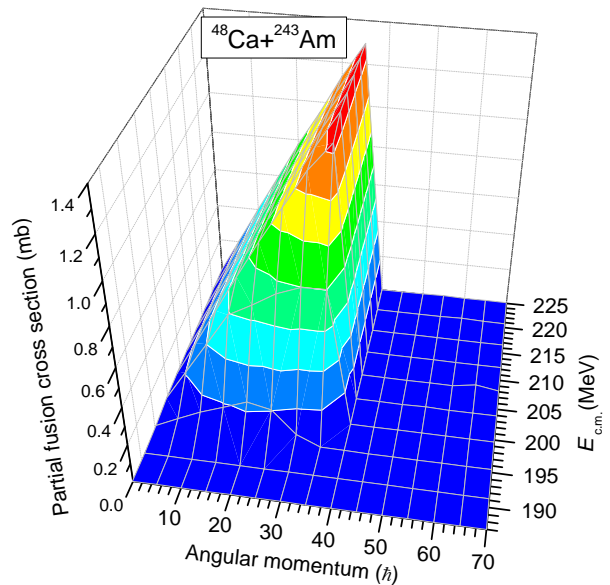


FIG. 4. (Color online) The partial fusion cross section calculated in this work for the $^{48}\text{Ca}+^{243}\text{Am}$ reaction as a function of the collision energy $E_{c.m.}$ and orbital angular momentum L .

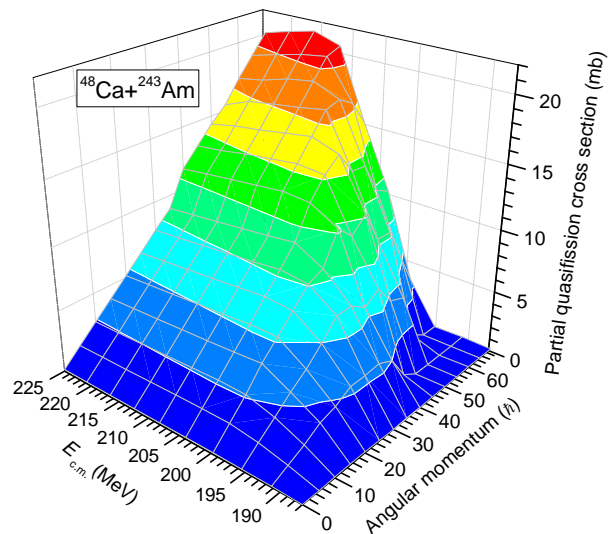


FIG. 5. (Color online) The same as in Fig. 4 but for the quasifission cross section.

have been calculated for the wide range of the excitation energy of the compound nucleus. The theoretical results of this work is compared with the experimental data obtained in Refs. [6–8]. The comparison of the experimental data and theoretical results of the ER cross sections, as well as the theoretical results obtained in this work for the complete fusion, quasifission and fast fission processes are presented in Fig. 7. It is seen that the agreement between theoretical and experimental results for the 2n, 3n and 4n channels of the ER formation are

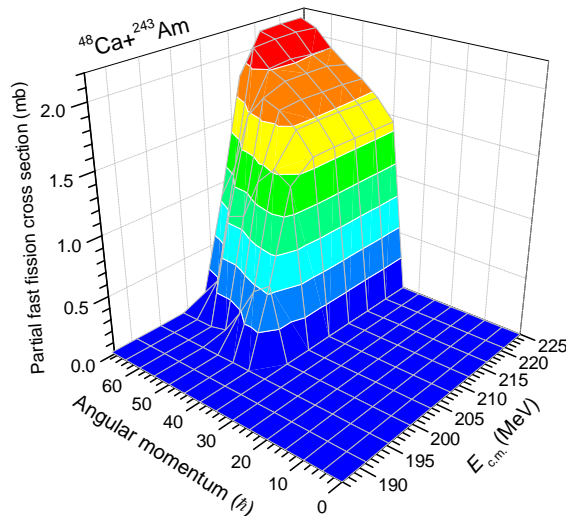


FIG. 6. (Color online) The same as in Fig. 4 but for the fast fission cross section.

good. The values of the E_{CN}^* are estimated only theoretically by the use of the reaction energy balance Q_{gg} and collision energy $E_{c.m.}$: $E_{CN}^* = E_{c.m.} + Q_{gg}$, where $Q_{gg} = B_P(^{48}\text{Ca}) + B_T(^{243}\text{Am}) - B_{CN}(^{291}\text{Mc})$ depends on the binding energies (B_P and B_T) of the colliding nuclei and being formed compound nucleus ($B_{CN}(^{291}\text{Mc})$). The value of $B_{CN}(^{291}\text{Mc})$ is equal to 178.97 and 182.99 MeV in Refs. [59] and [72], respectively. This means that the value of E_{CN}^* corresponding to the given value $E_{c.m.}$ may be different in dependence on what the mass table is used by the authors of papers. In Ref. [8] the spreading E_{CN}^* is presented in their Table 1. We have presented the ranges for the E_{CN}^* values at the given beam energies E_{lab}^* in Table II. As it is seen from the Table II and Fig. 7 there is an uncertainty in estimation of the CN excitation energy with the width about 4 MeV. The absolute values of the theoretical and experimental data are in a good agreement.

The successful application of the method presented in Section 3 to the description of the ER cross sections of the $^{48}\text{Ca} + ^{243}\text{Am}$ allows us to cal-

TABLE II. Laboratory-frame beam energies E_{lab} in the middle of the target layers, in the mass-centre system collision energies $E_{c.m.}$, resulting excitation energy intervals, E_{CN}^* values calculated by the use of the mass tables in [59] and [72], respectively.

E_{lab} (MeV)	$E_{c.m.}$ (MeV)	CN excitation energy intervals (MeV) [7, 8]	E_{CN}^* [59] (MeV)	E_{CN}^* [72] (MeV)
239.8	200.25	31.1—35.3	34.23	30.21
240.5	200.83	31.4—36.2	34.81	30.79
241.0	201.25	32.0—36.4	35.23	31.21
243.4	203.25	34.0—38.3	37.23	33.21
248.1	207.18	38.0—42.3	41.16	37.14
253.8	211.94	42.5—47.2	45.92	41.90

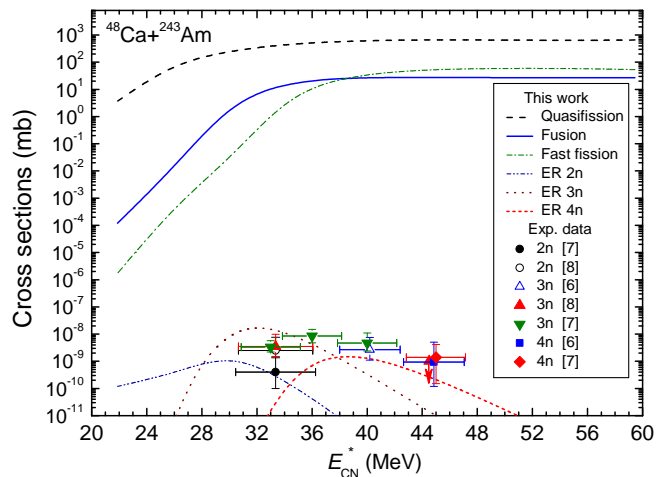


FIG. 7. (Color online) Theoretical cross sections of the quasifission (dashed black curve), complete fusion (solid blue curve), fast fission (dot-dashed green curve) and ER formation in 2n (thin dot-dashed violet curve), 3n (thin wine dotted curve) and 4n (thin short dashed red curve) channels, as well as the experimental data of the ER formation in the same channels as a function of the CN excitation energy: the 2n channel data labelled by solid circles have been obtained from Refs. [7] and [8], respectively; the 3n channel data shown by the open up and down triangles were obtained from Refs. [6] and [8]; the 4n channel data shown by the square and diamond were obtained from Refs. [6] and [7], respectively.

culate the ER cross sections of the $^{54}\text{Cr} + ^{243}\text{Am}$ which leads to formation of the SHE with the charge number $Z=119$.

In Fig. 8, the partial fusion cross section (in units μb) calculated by Eq. (17) for the $^{54}\text{Cr} + ^{243}\text{Am}$ reaction is presented as a function of the CN excitation energy E_{CN}^* and orbital angular momentum ℓ . The sharp decreasing its values at $\ell > 35$ is related with the disappear of the fission barrier of the compound nucleus $^{297}119$. This phenomenon is taken into account by Eqs. (24) and (25) which give a decrease of the fission barrier B_f by increase of the excitation energy and angular momentum of the compound nucleus formed at complete fusion of colliding nuclei. The mononucleus (the DNS being transformed into compound nucleus) with the angular momentum distributions in the range larger than $\ell > 35$ undergoes to fast fission and its products can have mass distributions as ones of fusion-fission and/or quasifission. The dependence of the fusion probability P_{CN} on the orbital angular momentum for the values of the CN excitation energies $E_{CN}^* = 32.0, 40.2, 48.4$ and 52.6 MeV is shown in Fig. 9. The increase of the P_{CN} values by the increase of the collision energy is due to the increase of DNS excitation energy and its decreasing by the increase of the angular momentum is caused by the increase of the intrinsic fusion barrier B_{fus}^* as a function of the angular momentum. The decrease of the fission

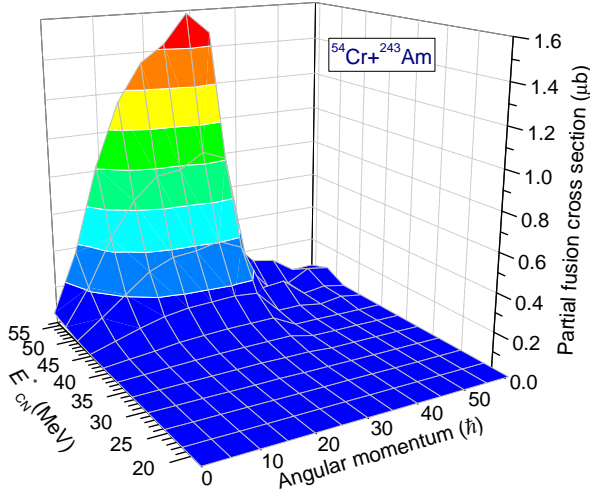


FIG. 8. (Color online) The partial fusion cross section calculated in this work for the $^{54}\text{Cr} + ^{243}\text{Am}$ reaction as a function of the collision energy $E_{\text{c.m.}}$ and orbital angular momentum L .

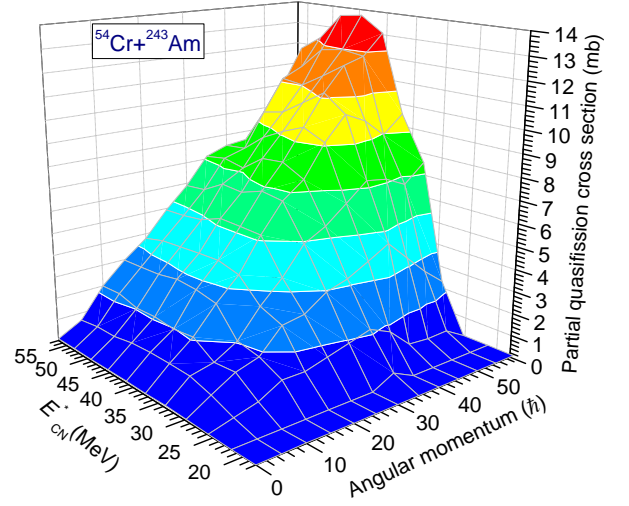


FIG. 10. (Color online) The same as in Fig. 8 but for the quasifission cross section.

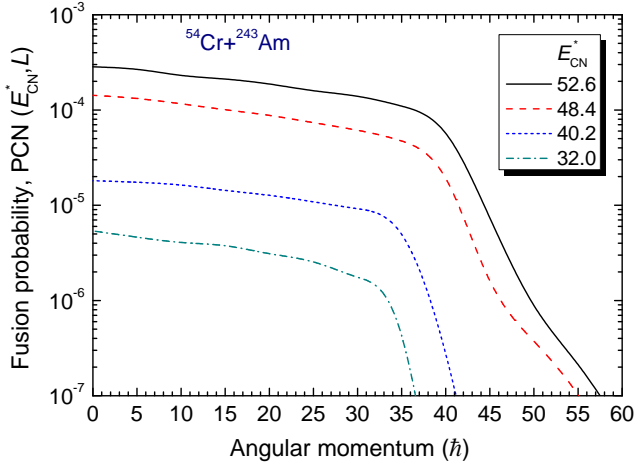


FIG. 9. (Color online) The dependence of the fusion probability $P_{\text{CN}}(E_{\text{c.m.}}, L)$ on the orbital angular momentum for the values of the CN excitation energies $E_{\text{CN}}^* = 32.0, 40.2, 48.4$ and 52.6 MeV for the $^{54}\text{Cr} + ^{243}\text{Am}$ reaction.

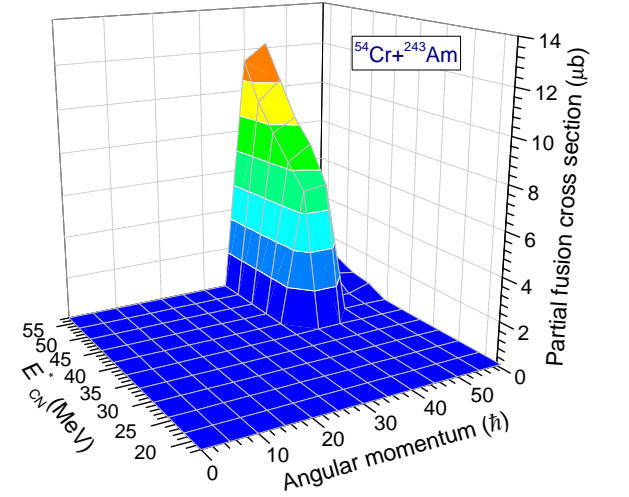


FIG. 11. (Color online) The same as in Fig. 8 but for the fast fission cross section.

barrier leads to the strong decrease of P_{CN} since the being formed CN becomes less stable against fission. Very small values of the fusion cross section obtained for the $^{54}\text{Cr} + ^{243}\text{Am}$ in comparison with the ones calculated for the $^{48}\text{Ca} + ^{243}\text{Am}$ reactions are due to large values of the intrinsic fusion barrier B_{fus}^* for the former reaction, as well as the decrease of the quasifission barrier due to increase the charge number $Z = 24$ of ^{54}Cr against the charge number $Z = 20$ of ^{48}Ca in the entrance channel.

The partial cross section of the quasifission process (see Fig. 10) is much larger in comparison with the cross sections of the fusion and fast fission products since according to the results presented in Figs. 8 and 11. This means the yield of the quasifission products is dominant among

the yield of the products of the other mechanisms. Here we should note that the unit of the quasifission cross section is in millibarn (mb) in Fig. 10 while the units of the fusion (Fig. 8) and fast fission cross sections (Fig. 11) are presented in microbarn μb . To answer on the question about reasons calling the difference between the cross sections of the complete fusion of the $^{48}\text{Ca} + ^{243}\text{Am}$ and $^{54}\text{Cr} + ^{243}\text{Am}$ reactions we have presented in Figs. 12 and 13 the comparisons of the intrinsic fusion B_{fus}^* and quasifission B_{qf} barriers, respectively, calculated in this work. It is seen from Fig. 12 that the hindrance to complete fusion is stronger in the $^{54}\text{Cr} + ^{243}\text{Am}$ reaction in comparison with the case of the $^{48}\text{Ca} + ^{243}\text{Am}$ reaction since the values of B_{fus}^* for the former reaction are about two times larger the ones for the latter reaction. At the same time the values of the B_{qf} for the $^{54}\text{Cr} + ^{243}\text{Am}$ reac-

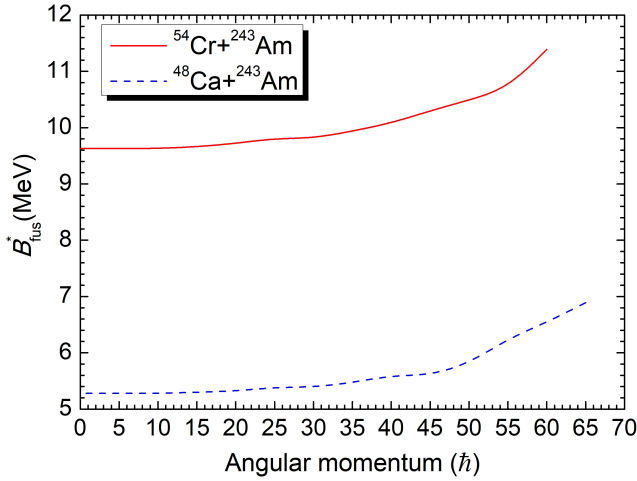


FIG. 12. (Color online) Comparison of the results for the intrinsic fusion barrier B_{fus}^* for the $^{54}\text{Cr}+^{243}\text{Am}$ and $^{48}\text{Ca}+^{243}\text{Am}$ reactions calculated in this work as a function of the DNS angular momentum (L).

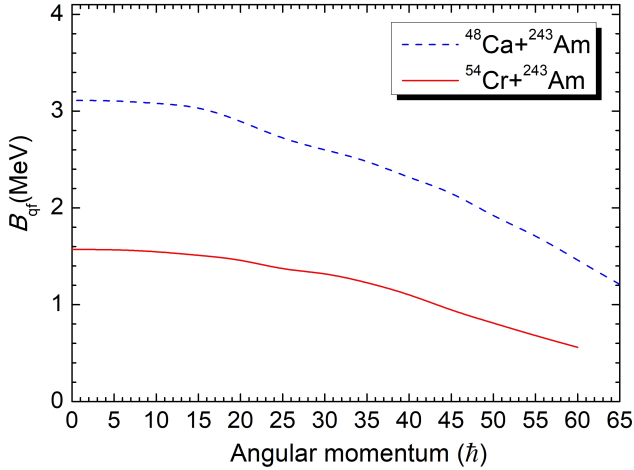


FIG. 13. (Color online) Comparison of the results for the quasifission barrier B_{qf} for the $^{54}\text{Cr}+^{243}\text{Am}$ and $^{48}\text{Ca}+^{243}\text{Am}$ reactions calculated in this work as a function of the DNS angular momentum (L).

tion are smaller about two times in comparison with the case of the $^{48}\text{Ca}+^{243}\text{Am}$ reaction. Certainly, the DNS lifetime formed in the $^{48}\text{Ca}+^{243}\text{Am}$ reaction is longer it has more opportunity to be transformed into compound nucleus.

The total cross sections for the $^{54}\text{Cr}+^{243}\text{Am}$ reaction summarized over values of the angular momentum are presented in Fig. 14. It is seen that the cross sections of the complete fusion and fast fission are comparable.

The excitation functions of the 2n, 3n and 4n de-excitation channels are presented in Fig. 14 and separately in Fig. 15. The maximum of the evaporation residue cross section predicted around the excitation energy of compound nucleus $E_{\text{CN}}^* = 32\text{--}35$ MeV and 3n

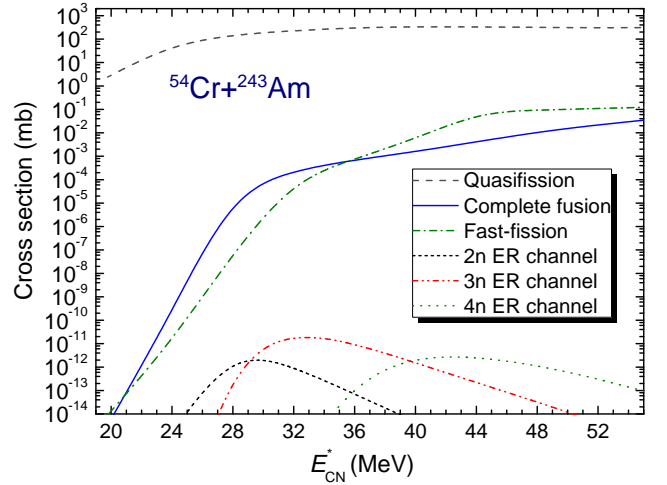


FIG. 14. (Color online) Theoretical cross sections of the quasifission (dashed black curve), complete fusion (solid blue curve), fast fission (dot-dashed green curve) and ER formation in 2n (thin short dashed black curve), 3n (thin dash-double dotted red curve) and 4n (thin dotted green curve) channels cross sections calculated in this work as a function of E_{CN}^* for the $^{54}\text{Cr}+^{243}\text{Am}$ reaction.

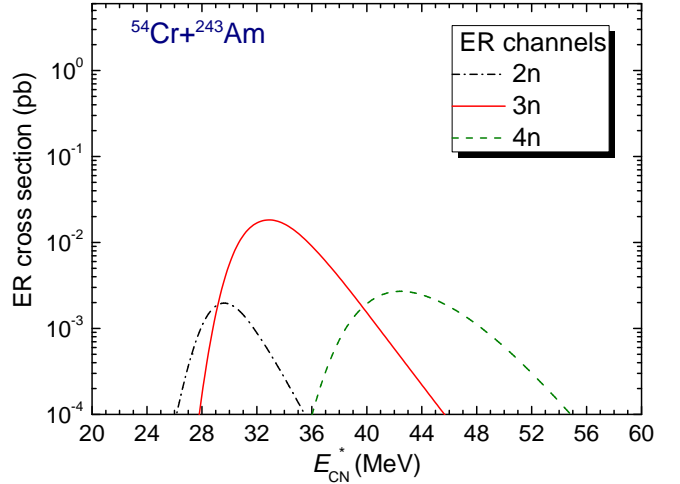


FIG. 15. (Color online) The expected ER cross section for producing superheavy element 119 via $^{54}\text{Cr}+^{243}\text{Am}$ reaction in the 2n (dot-dashed black curve), 3n (solid red curve) and 4n (dashed green curve) channels.

channel of the evaporation residues events dominates. Maximum value of its cross section is about 25 fb and the corresponding events can be observed in the Super-Heavy Element Factory (DC-280 cyclotron) of the Flerov Laboratory of Nuclear Reaction (JINR, Dubna) [73]. In Ref. [48], the predicted cross section for the 3n channel of ER for the $^{53}\text{Cr}+^{243}\text{Am}$ reaction is 0.95 pb at the excitation energy $E_{\text{CN}}^* = 33$ MeV. Looking at these values we can conclude that our prediction is intermediate between them. Authors of Ref. [49] have predicted the maximum value of the ER cross section of the 3n channel for the

$^{54}\text{Cr}+^{243}\text{Am}$ reaction for 1.82 fb.

V. CONCLUSION

The peculiarities of the processes in the heavy ion reactions, which can lead to formation of superheavy elements, have been explored by the methods of the DNS concept. The formation probability of the DNS at capture stage of the heavy ion collisions is calculated by solution of the equation of motions for the relative distance and orbital angular momentum at the given collision energy $E_{\text{c.m.}}$ for the $^{48}\text{Ca}+^{243}\text{Am}$ and $^{54}\text{Cr}+^{243}\text{Am}$ reactions. An orientation angle of the symmetry axis of the deformed nucleus and vibrational states of the spherical nucleus are included in calculation of the partial capture cross sections.

The transformation probability of the DNS into compound nucleus is calculated by the estimations of the branching ratio of the nuclear level densities on the saddle point to the complete fusion and on the Coulomb barrier of the nucleus-nucleus interaction of the potential energy surface. The results of calculation have shown the quasifission is dominant channel of the capture events for the both reactions. It has very large cross sections for the $^{54}\text{Cr}+^{243}\text{Am}$ reaction. The probability of the observation of the new superheavy element $Z=119$ enough small and it is near border of the experimental possibilities. Our calculations have given the result about 0.025 pb for the evaporation residue cross section at the excitation energy

$E_{\text{CN}}^*=32$ MeV for the 3n- channel. To show the dependence of the all stages of the reaction chain at formation of superheavy element on the DNS angular momentum the partial cross sections of the quasifission, complete fusion and fast fission processes are presented for the wide range of the excitation energy of the compound nucleus. The reasons leading to the dominance of the quasifission over complete fusion and fast fission processes and causing strong difference in the cross sections of complete fusion for the $^{48}\text{Ca}+^{243}\text{Am}$ and $^{54}\text{Cr}+^{243}\text{Am}$ reactions are the values of the intrinsic fusion barrier calculated for the wide range of the DNS angular momentum. It is demonstrated that the values of the intrinsic fusion barrier for the $^{54}\text{Cr}+^{243}\text{Am}$ reaction is about two times higher than ones obtained for the $^{48}\text{Ca}+^{243}\text{Am}$ reaction. Therefore, a hindrance to complete fusion is stronger for the reactions with the more massive projectile ^{54}Cr . The DNS formed in the $^{54}\text{Cr}+^{243}\text{Am}$ reaction is less stable in comparison with the one formed in the $^{48}\text{Ca}+^{243}\text{Am}$ reaction since the quasifission barriers for the DNS calculated for the former reaction is smaller than the ones found for the latter reaction.

ACKNOWLEDGMENTS

The authors are grateful to the Ministry of Innovative Development of Uzbekistan (M.I.D.U.), for financial support in the implementation of this research work.

-
- [1] S. Hofmann and G. Münzenberg, *Rev. Mod. Phys.* **72**, 733 (2000).
- [2] P. Armbruster, *Annu. Rev. Nucl. Part. Sci.* **50**, 411 (2000).
- [3] K. Morita *et al.*, *J. Phys. Soc. Jpn.* **73**, 2593 (2004).
- [4] Y. T. Oganessian *et al.*, *Phys. Rev. C* **74**, 044602 (2006).
- [5] Y. T. Oganessian, *J. Phys. G: Nucl. Part. Phys.* **34**, R165 (2007).
- [6] Y. T. Oganessian *et al.*, *Phys. Rev. C* **72**, 034611 (2005).
- [7] Y. T. Oganessian *et al.*, *Phys. Rev. Lett.* **108**, 022502 (2012).
- [8] Y. T. Oganessian *et al.*, *Phys. Rev. C* **87**, 014302 (2013).
- [9] G. Münzenberg and K. Morita, *Nucl. Phys. A* **944**, 3 (2015).
- [10] J. Dvorak *et al.*, *Phys. Rev. C* **79**, 037602 (2009).
- [11] R. Graeger *et al.*, *Phys. Rev. C* **81**, 061601 (2010).
- [12] K. Nishio *et al.*, *Phys. Rev. C* **86**, 034608 (2012).
- [13] N. T. Brewer *et al.*, *Phys. Rev. C* **98**, 024317 (2018).
- [14] Y. T. Oganessian *et al.*, *Phys. Rev. C* **79**, 024603 (2009).
- [15] S. Hofmann *et al.*, in *GSI Scientific Report 2011 [GSI Report 2012-1]*, Vol. 2012-1, edited by G. Katrin (GSI, Darmstadt, 2012) p. 205.
- [16] J. Töke *et al.*, *Nucl. Phys. A* **440**, 327 (1985).
- [17] R. du Rietz, E. Williams, D. J. Hinde, M. Dasgupta, M. Evers, C. J. Lin, D. H. Luong, C. Simenel, and A. Wakhle, *Phys. Rev. C* **88**, 054618 (2013).
- [18] M. G. Itkis *et al.*, *Nucl. Phys. A* **787**, 150 (2007).
- [19] I. M. Itkis *et al.*, *Phys. Rev. C* **83**, 064613 (2011).
- [20] E. M. Kozulin *et al.*, *Phys. Rev. C* **94**, 054613 (2016).
- [21] G. Giardina, G. Mandaglio, A. Nasirov, A. Anastasi, F. Curciarello, and G. Fazio, *Nucl. Phys. A* **970**, 169 (2018).
- [22] K. Banerjee *et al.*, *Phys. Rev. Lett.* **122**, 232503 (2019).
- [23] G. Adamian, N. Antonenko, W. Scheid, and V. Volkov, *Nucl. Phys. A* **627**, 361 (1997).
- [24] C. Shen, Y. Abe, D. Boilley, G. Kosenko, and E. Zhao, *Int. J. Mod. Phys. E* **17**, 66 (2008).
- [25] V. Zagrebaev and W. Greiner, *Phys. Rev. C* **78**, 034610 (2008).
- [26] N. Wang, J.-Q. Li, and E.-G. Zhao, *Phys. Rev. C* **78**, 054607 (2008).
- [27] Z. H. Liu and J.-D. Bao, *Phys. Rev. C* **80**, 054608 (2009).
- [28] A. K. Nasirov, G. Giardina, G. Mandaglio, M. Mangano, F. Hanappe, S. Heinz, S. Hofmann, A. I. Muminov, and W. Scheid, *Phys. Rev. C* **79**, 024606 (2009).
- [29] R. Smolańczuk, *Phys. Rev. C* **81**, 067602 (2010).
- [30] N. Wang, J. Tian, and W. Scheid, *Phys. Rev. C* **84**, 061601 (2011).
- [31] K. Siwek-Wilczyńska, T. Cap, M. Kowal, A. Sobczewski, and J. Wilczyński, *Phys. Rev. C* **86**, 014611 (2012).
- [32] N. Wang, E.-G. Zhao, and W. Scheid, *Phys. Rev. C* **89**, 037601 (2014).
- [33] X. J. Bao, Y. Gao, J. Q. Li, and H. F. Zhang, *Phys. Rev. C* **91**, 011603 (2015).

- [34] Z.-H. Wu, L. Zhu, F. Li, X.-B. Yu, J. Su, and C.-C. Guo, *Phys. Rev. C* **97**, 064609 (2018).
- [35] M. Huang, Z. Zhang, Z. Gan, X. Zhou, J. Li, and W. Scheid, *Phys. Rev. C* **84**, 064619 (2011).
- [36] N. Antonenko, E. Cherepanov, A. Nasirov, V. Permjakov, and V. Volkov, *Phys. Lett. B* **319**, 425 (1993).
- [37] N. V. Antonenko, E. A. Cherepanov, A. K. Nasirov, V. P. Permjakov, and V. V. Volkov, *Phys. Rev. C* **51**, 2635 (1995).
- [38] A. K. Nasirov, A. I. Muminov, R. K. Utamuratov, G. Fazio, G. Giardina, F. Hanappe, G. Mandaglio, M. Manganaro, and W. Scheid, *Eur. Phys. J. A* **34**, 325 (2007).
- [39] A. Nasirov, A. Fukushima, Y. Toyoshima, Y. Aritomo, A. Muminov, S. Kalandarov, and R. Utamuratov, *Nucl. Phys. A* **759**, 342 (2005).
- [40] A. K. Nasirov, G. Mandaglio, G. Giardina, A. Sobiczewski, and A. I. Muminov, *Phys. Rev. C* **84**, 044612 (2011).
- [41] J. Hong, G. G. Adamian, and N. V. Antonenko, *Phys. Rev. C* **94**, 044606 (2016).
- [42] G. Mandaglio, G. Giardina, A. K. Nasirov, and A. Sobiczewski, *Phys. Rev. C* **86**, 064607 (2012).
- [43] X. J. Bao, Y. Gao, J. Q. Li, and H. F. Zhang, *Phys. Rev. C* **92**, 034612 (2015).
- [44] N. Wang, E.-G. Zhao, W. Scheid, and S.-G. Zhou, *Phys. Rev. C* **85**, 041601 (2012).
- [45] Z.-H. Liu and J.-D. Bao, *Phys. Rev. C* **87**, 034616 (2013).
- [46] L. Zhu, W.-J. Xie, and F.-S. Zhang, *Phys. Rev. C* **89**, 024615 (2014).
- [47] X. Bao, S. Guo, H. Zhang, and J. Li, *J. Phys. G: Nucl. Part. Phys.* **43**, 125105 (2016).
- [48] F. Li, L. Zhu, Z.-H. Wu, X.-B. Yu, J. Su, and C.-C. Guo, *Phys. Rev. C* **98**, 014618 (2018).
- [49] X.-J. Lv, Z.-Y. Yue, W.-J. Zhao, and B. Wang, *Phys. Rev. C* **103**, 064616 (2021).
- [50] A. K. Nasirov, A. I. Muminov, G. Giardina, and G. Mandaglio, *Phys. At. Nucl.* **77**, 881 (2014).
- [51] A. J. Sierk, *Phys. Rev. C* **33**, 2039 (1986).
- [52] G. Fazio, G. Giardina, F. Hanappe, G. Mandaglio, M. Manganaro, A. I. Muminov, A. K. Nasirov, and C. Saccà, *J. Phys. Soc. Jpn.* **77**, 124201 (2008).
- [53] A. Nasirov, K. Kim, G. Mandaglio, G. Giardina, A. Muminov, and Y. Kim, *Eur. Phys. J. A* **49**, 147 (2013).
- [54] K. Kim, Y. Kim, A. K. Nasirov, G. Mandaglio, and G. Giardina, *Phys. Rev. C* **91**, 064608 (2015).
- [55] A. Nasirov, B. Kayumov, and Y. Oh, *Nucl. Phys. A* **946**, 89 (2016).
- [56] G. Fazio, G. Giardina, A. Lamberto, R. Ruggeri, C. Saccà, R. Palamara, A. I. Muminov, A. K. Nasirov, U. T. Yakhshiev, F. Hanappe, T. Materna, and L. Stuttgé, *J. Phys. Soc. Jpn.* **72**, 2509 (2003).
- [57] E. C. Kemble, *Phys. Rev.* **48**, 549 (1935).
- [58] G. Audi and A. Wapstra, *Nucl. Phys. A* **595**, 409 (1995).
- [59] P. Moller, J. Nix, W. Myers, and W. Swiatecki, *At. Data Nucl. Data Tables* **59**, 185 (1995).
- [60] H. Q. Zhang, C. L. Zhang, C. J. Lin, Z. H. Liu, F. Yang, A. K. Nasirov, G. Mandaglio, M. Manganaro, and G. Giardina, *Phys. Rev. C* **81**, 034611 (2010).
- [61] H. Esbensen, *Nucl. Phys. A* **352**, 147 (1981).
- [62] S. Raman, C. Nestor, and P. Tikkanen, *At. Data Nucl. Data Tables* **78**, 1 (2001).
- [63] R. Spear, *At. Data Nucl. Data Tables* **42**, 55 (1989).
- [64] H. Lü, A. Marchix, Y. Abe, and D. Boilley, *Comput. Phys. Commun.* **200**, 381 (2016).
- [65] V. Weisskopf, *Phys. Rev.* **52**, 295 (1937).
- [66] N. Bohr and J. A. Wheeler, *Phys. Rev.* **56**, 426 (1939).
- [67] M. Grossjean and H. Feldmeier, *Nucl. Phys. A* **444**, 113 (1985).
- [68] D. L. Hill and J. A. Wheeler, *Phys. Rev.* **89**, 1102 (1953).
- [69] J. Zhang, C. Wang, and Z. Ren, *Nucl. Phys. A* **909**, 36 (2013).
- [70] F. A. Ivanyuk and K. Pomorski, *Phys. Rev. C* **79**, 054327 (2009).
- [71] A. Ignatyuk, G. Smirenkin, and A. Tishin, *Yadernaya Fizika* **21**, 485 (1975).
- [72] I. Muntian, Z. Patyk, and A. Sobiczewski, *Phys. At. Nucl.* **66**, 1015 (2003).
- [73] <http://flerovlab.jinr.ru/she-factory/> (2021).